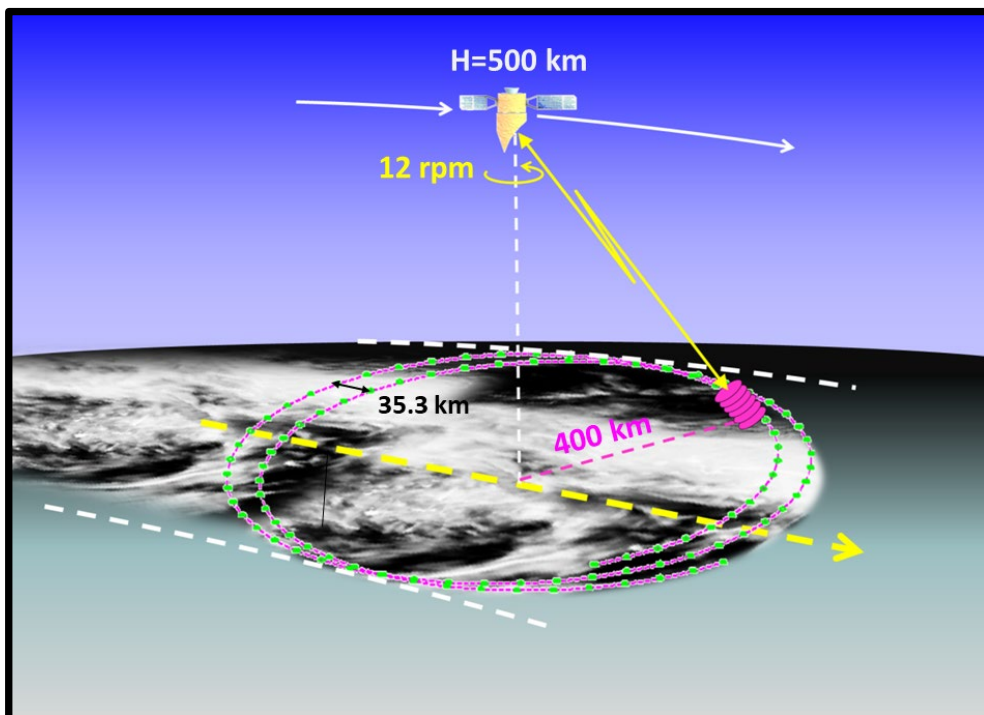


WIVERNEX-UK

Technical Assistance to Earth Explorer 11 WIVERN Phase 0 Campaigns Experiment in the UK

FINAL REPORT

ESA Contract no. 4000139702/22/NL/FF/ab



University of
Reading



Science and
Technology
Facilities Council

Authors:

A.J. Illingworth, J.C. Nicol, R. Thompson, University of Reading

C. J. Walden, R. Reeves, STFC Chilbolton Observatory

A Battaglia, Politecnico Torino

Document version	Date	Modifications and comments
1.0	32/12/2023	First version

TABLE OF CONTENTS

1.	CAMPAIGN OBJECTIVES.....	4
2.	CAMPAIGN LOCATION.....	4
3.	RADAR INSTRUMENTATION AND OPERATION.....	5
3.1	<i>The 94 GHz Galileo cloud radar</i>	5
3.2	<i>The 35 GHz Copernicus cloud radar</i>	7
3.3	<i>The 3 GHz Chilbolton Advanced Meteorological Radar (CAMRa)</i>	8
4.	DATA ACQUISITION REPORT.....	9
	PHASE 1: FEBRUARY-APRIL 2023	9
	PHASE 2: MAY-JULY 2023	10
	PHASE 3: NOT ACHIEVED	10
	DATA PROCESSING LEVELS	11
5.	ANALYSIS.....	12

1. CAMPAIGN OBJECTIVES

This campaign was designed to extend the Chilbolton ground measurement record with the following objectives:

Objective 1: Analysis of observations in zenith orientation and at 42° incidence of ghost echoes, and validation of correction algorithms. This aims to address whether the reflectivity bias caused by these occasional ghosts can be removed using alternate H-V, V-H pulses.

Objective 2: Validation of rain-rate retrieval algorithms.

Objective 3: Exploitation of campaign data to improve the E2E modelling (carried out by PoT)

2. CAMPAIGN LOCATION

The Chilbolton Observatory, located in Southern England, is home to a suite of atmospheric radar facilities operated by the Science and Technology Facilities Council (a member council of UK Research and Innovation, UKRI) as part of the National Centre for Atmospheric Science (NCAS). These furnish the research community with long-term observational datasets, as well as supporting intensive campaigns, often coordinated with research aircraft. Radar instrumentation is augmented by the colocation of a comprehensive combination of lidars, radiometers, and a wide variety of in-situ meteorological sensors.

Chilbolton has been involved in millimetre-wave radar observations of clouds for more than two decades. It was one of the pilot sites for the EU FP5 Cloudnet project, and a cloud-profiling station has been in operation at Chilbolton for more than 15 years, exploiting the 35 and 94 GHz radars on site. This station contributes to ongoing international capability as part of the Aerosol Clouds and Trace gases Research Infrastructure (ACTRIS).



Figure 1: Aerial view of the Chilbolton site

3. RADAR INSTRUMENTATION AND OPERATION

Three radars (see Figure 2) were intended to be involved in the ground-based campaign, maintained and operated by STFC (as part of UKRI) in partnership with NCAS. For completeness they are specified here, although for reasons explained later in this report only data from the 94 GHz Galileo radar were used.

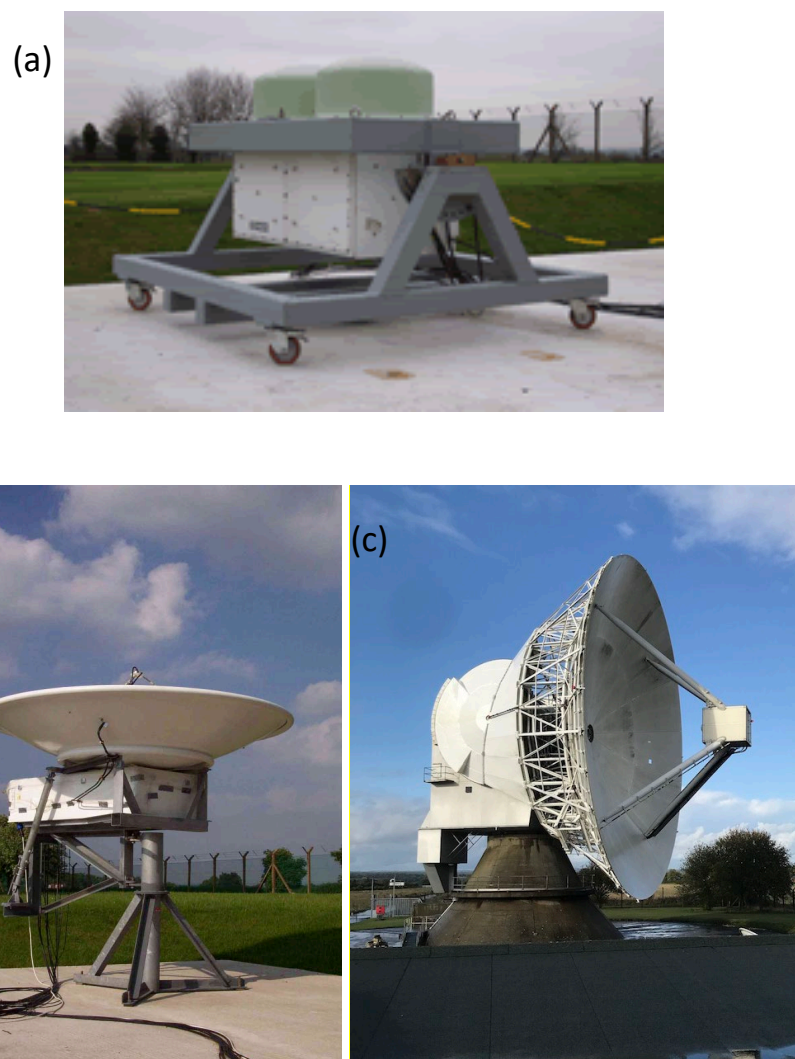


Figure 2: Chilbolton radars to be used in this campaign – (a) 94GHz Galileo radar, and (b) 35GHz Copernicus radar, (c) 3GHz radar (CAMRa) on the 25 m antenna.

3.1 THE 94 GHz GALILEO CLOUD RADAR

The Galileo radar is a fully coherent W-band dual-polarisation pulsed Doppler radar designed for observations of cloud microphysics and climatology. It is based on a crystal-controlled reference and synthesisers plus frequency multiplier chains to generate all necessary RF and

system timing signals. The transmitter is based on a high-power pulsed millimetre-wave extended interaction klystron amplifier (EIKA) tube manufactured by CPI (Communications and Power Industries, Canada Inc.), while the receiver is a single-conversion super-heterodyne. The transmitter incorporates a polarisation switch to allow sequences of H and V polarised pulses to be transmitted and there are separate IF receiver chains for each polarisation. A pair of mutually aligned dishes in a bistatic configuration form the radar antenna to provide sufficient transmit-receive isolation. Further details are given in Table 1.

Table 1: Specification of 94 GHz Galileo radar

Parameter	Value/comment
Operating frequency	94.008 GHz
Transmit polarisation	Programmable sequences of H- and V-polarised pulses
Receive polarisation	Simultaneous co- and cross-polar
Transmit power	1.5 kW peak pulse
Range resolution	60 m
Pulse repetition frequency	6250 Hz
Maximum unambiguous velocity	4.98 ms ⁻¹
Antenna type	Two Cassegrain-fed parabolic dishes (bistatic)
Diameter	0.46 m
Gain	50.0 dBi
Beam width	0.49° (FWHM, -3 dB one-way)

During 2022 the high voltage power supply for this radar was shipped to CPI for fault investigation and underwent a subsequent repair. Additionally, the EIKA was replaced, as the previous one had been in operation since 2011 and was showing a fall-off in achievable peak power. The new EIKA has a maximum duty cycle of 3% and has been operating since mid-December 2022. Compared with the performance of the radar before the fault developed in February 2022 this has resulted in an increase of approximately 1dB in peak transmitted power.

The configuration and operation of this instrument was key to achieving the objectives of the campaign. Specifically, in order to evaluate pulse-pair velocity estimates the radar needed to have options for configuring selection and dynamic switching of pulse modes. This capability was previously established as part of the WIVERN-2 project (ESA contract 4000130864/20/NL/CT), but pulse-pair processing was hard coded into the data acquisition software. To meet present campaign objectives, it was desirable to allow maximum flexibility in the analysis of acquired data. To this end it was decided that recording of individual values of I and Q at each gate would be used, and that spectral and pulse-pair processing would be performed offline. Further software development work was carried out by STFC during

December 2022 to permit selection of alternating modes of pulse transmission in the I/Q acquisition code.

The data were collected with alternating single- and double-pulse configuration. The single pulse rays were the conventional Doppler as used at the ground with a folding velocity of 5 m/s and provide the “truth”, whereas the double-pulse rays had the WIVERN configuration with the high folding velocity of 40 m/s. Each ray was of 1-sec. duration (6144 pulses) with alternating polarization. The single-pulse rays alternate between H and V every 160 μ s and the double-pulse rays alternate between HV and VH every 160 μ s (HV designates an H pulse followed by a V pulse with a 20 μ s separation). Data were recorded into NetCDF-3 files every 3 minutes (each incorporating 180 rays).

The offline pulse-pair processing that has been implemented by the University of Reading initially subtracts the mean I and Q values for each one second ray in each channel (H and V) for each file. This removes the DC offsets at baseband. The data are then separated into single- and double-pulse rays. Each ray is also separated into H and V based on the polarization of the transmitted pulse (leading transmitted pulse in the case of the double-pulse rays). For each polarization, the power is calculated in the co-polar and cross-polar channels and the noise level is determined based on the mean power in the furthest 20 range gates (between about 10.5-11.6 km).

3.2 THE 35 GHz COPERNICUS CLOUD RADAR

The Copernicus radar is a fully coherent Ka-band dual-polarisation pulse-compression Doppler radar designed for observations of cloud microphysics and climatology. It employs a crystal-controlled reference and frequency synthesisers to generate all necessary RF and system timing signals. The transmitter is based on a flexible programmable waveform generator driving a high-power pulsed millimetre-wave klystron amplifier tube. The receiver is a dual-channel, double-conversion superheterodyne with separate IF chains for simultaneous co-polar and cross-polar measurements. A dual-polarisation antenna and a fast, latching circulator-based, transmit polarisation switch complete the design. The radar provides real-time measurement and display of the full Doppler spectrum, the spectral moments and the polarimetric parameters. Time-series data are also available for more detailed off-line analysis. Further details of the radar are given in Table 2.

Table 2: Specification of 35 GHz Copernicus radar

Parameter	Value/comment
Operating frequency	34.960 GHz
Transmit polarisation	Horizontal and vertical pulse-to-pulse switching
Receive polarisation	Co- and cross-polar
Transmit power	1.5 kW peak pulse
Range resolution	60 m

Pulse repetition frequency	5000 Hz
Maximum unambiguous velocity	10.72 ms ⁻¹
Antenna type	Prime-focus fed parabolic dish
Diameter	2.4 m
Gain	55.9 dBi
Beam width	0.25° (FWHM, -3 dB one-way)

During 2022 the data acquisition computer for this radar was upgraded to a 64-bit system. Porting of code to this new system was completed in November 2022.

As in previous Chilbolton WIVERN studies, to allow maximum flexibility in data analysis the data acquisition plan was record I and Q values at each range gate, with the data being stored in binary format files once per minute. These files were then intended to be post-processed to generate NetCDF format files for further analysis.

3.3 THE 3 GHz CHILBOLTON ADVANCED METEOROLOGICAL RADAR (CAMRA)

The S-band radar (CAMRa) is a dual-polarisation Doppler radar based on a fully steerable 25 m diameter dish antenna, a magnetron transmitter, a dual-channel super-heterodyne receiver, and a hybrid analogue-digital signal processor. The radar uses a digital signal processing scheme to achieve coherent-on-receive operation. The radar transmits alternately horizontally and vertically polarised pulses and receives both co-polar and cross-polar returns. This approach permits real-time measurement and display of Z, ZDR, LDR, Doppler velocity and spectral width, ϕ_{DP} , and ρ_{HV} . For more detailed studies, full time-series measurements of I and Q are also possible over a large number of range gates and transmitted pulses.

Table 3: Specification of the 3 GHz CAMRa radar

Parameter	Value/comment
Operating frequency	3.0765 GHz
Transmit polarisation	Horizontal and vertical pulse-to-pulse switching
Receive polarisation	Simultaneous co- and cross-polar
Transmit power	600 kW peak pulse
Range resolution	75 m
Pulse repetition frequency	612 Hz
Maximum unambiguous velocity	14.91 ms ⁻¹
Antenna type	Prime-focus fed parabolic dish
Diameter	25 m
Gain	53.5 dBi
Beam width	0.28° (FWHM, -3 dB one-way)

The operational configuration of this radar was intended to follow that used in the WIVERN-2 campaign in 2020/2021. This involves recording of I/Q time series, organised into rays of 3050 alternating H and V pulse pairs, stored as NetCDF-3 files every 15 minutes. The files store I and Q values from the limiting amplifiers in the receiver as well as recording the transmit I and Q for each pulse and co- and cross-polar reflectivity. The transmit and receive I/Q and reflectivity data are used in post-processing to produce a single time series for each polarisation.

4. DATA ACQUISITION REPORT

Data from the 35 GHz Copernicus radar and the 3 GHz radar (CAMRa) were intended to be acquired as part of Objective 2. These data would only have been relevant alongside the 94 GHz data, and as a result of the failure the 94 GHz radar, these measurements were not made.

Phase 1: February-April 2023

Observations were made with the 94 GHz Galileo radar in zenith-pointing geometry to observe ghosts and validate algorithms for subtracting the ghost reflectivity to leave the true reflectivity of the hydrometeors. The original schedule was extended into April to allow further cases to be acquired. Table 1 provides a summary.

Ghosts are frequently observed from the ground because of the large difference in range 1 and 4 km. Ghosts should result from the depolarising bright band. For a bright band at height 1 km, with a linear depolarisation ratio of -12 dB the ghosts will appear at a height of 4 km, the distance separating the H and V pulses for WIVERN. For a given reflectivity (dBZ) the return power at 1 km is 16 times (12 dB) greater than a target with the same Z at 4 km. If the target at 4 km has the same reflectivity as the bright band at 1 km, the magnitude of the ghost at 4 km will equal the signal from the hydrometeors at 4km, and the signal to ghost ratio will be unity (0 dB). From space the “r-squared” term is 1, as the range is about 650 km and the ghost would be 12 dB below the signal and be insignificant. This experimental was designed to test the algorithm to subtract the reflectivity of the ghost and also demonstrate that ghosts will be very rare for the WIVERN satellite.

Table 1: Phase 1 observations with the 94 GHz Galileo radar

CASE	First file date & time	Last file date & time
01	20230221-17:56:35	20230222-10:27:44
02	20230312-16:46:10	20230312-22:47:28
03	20230315-12:35:05	20230316-03:20:07
04	20230319-21:35:00	20230319-21:56:27
05	20230321-22:02:21	20230322-07:22:06
06	20230323-15:40:17	20230323-19:14:42
07	20230324-11:18:15	20230324-17:51:26
08	20230325-22:58:24	20230326-08:42:33
09	20230329-17:17:53	20230329-19:59:58
10	20230330-19:50:30	20230401-05:34:16

11	20230405-17:42:47	20230406-01:18:32
12	20230411-10:53:15	20230411-20:46:34
13	20230412-12:04:11	20230412-20:04:42
14	20230414-02:23:28	20230414-21:55:59

Phase 2: May-July 2023

Observations were made with the 94 GHz Galileo radar at an incidence angle of 42°. This phase was designed to evaluate ghost echoes and to verify that the correction algorithm works at the WIVERN angle. It also allowed comparison of the values of LDR with those found in the zenith geometry.

Due to additional Phase 1 observations the start of this phase was delayed by one month when compared with the Campaign Implementation Plan. In order to capture as many suitable rain events as possible, the duration of this phase was also extended, with the work being prioritised over that of Phase 3. This was justified on the basis that wind retrievals form the main mission capability for WIVERN.

Table 2: Phase 2 observations with the 94 GHz Galileo radar

CASE	First file date & time	Last file date & time
15	20230506-02:28:57	20230506-14:49:19
16	20230508-02:33:44	20230508-06:50:45
17	20230618-11:28:12	20230618-19:53:24
18	20230620-02:13:27	20230620-07:34:55
19	20230630-09:24:33	20230630-21:38:51
20	20230704-06:26:11	20230704-23:59:15

Phase 3: Not achieved

This phase was intended for evaluation of rain-rate retrievals, and the plan had been for observations with the 94 GHz Galileo radar, the 35 GHz Copernicus radar and the 3 GHz radar (CAMRa) all in zenith-pointing geometry. The aim had been to collect data during 15 days of wet weather. As noted above, there was a decision to prioritize slant-angle observations during June 2023.

Following discussions with ESA it had been intended to make some Phase 3 observations during June and July 2023. However, this was rendered unachievable due to a failure of the high-voltage power supply for the 94GHz Galileo radar. This occurred on the 8th July 2023. A similar failure in May 2023 was resolved with close guidance from the manufacturer (CPI). However, this new failure could not be resolved on site. The timeframe for repair extends into 2024. Figure 3 provides an overview of time-series data availability for the observations made during this campaign.

DATA PROCESSING LEVELS

A definition of the data processing levels is as follows.

Level 0: I and Q values at each range gate as recorded by each radar

For the 94 GHz radar the files are in NetCDF-3 format.

Level 1a: Processing to this level involves removing bias from the ADC samples of I and Q. Single estimates of I and Q for each transmit pulse are produced and stored in the output file. Campaign-specific metadata are also added before the files are finalised.

For the 94 GHz radar data it is important to keep track of the polarisation of each transmitted pulse. These data are captured at acquisition time and are preserved in the Level 1a files to assist with onward analysis.

Level 1b: Calibrated and quality-flagged I/Q time-series data. This is the format to be used for delivery of I/Q time-series.

Processing from Level 1a to Level 1b involves application of appropriate scale factors to account for calibration offsets, and addition of quality-control flags.

The L1b data format used is based on NetCDF4. With some minor differences that are clear from the embedded metadata, it aligns with that employed in previous WIVERN-2 work (under ESA Contract no. 4000130864/20/NL/CT) for which further information may be found at <https://wivern-chilbolton-utils.readthedocs.io>.

Level 2: Derived moments and pulse-pair velocities

STFC took responsibility for processing up to Level 1b. Further analysis and production of Level 2 data was performed by the University of Reading.

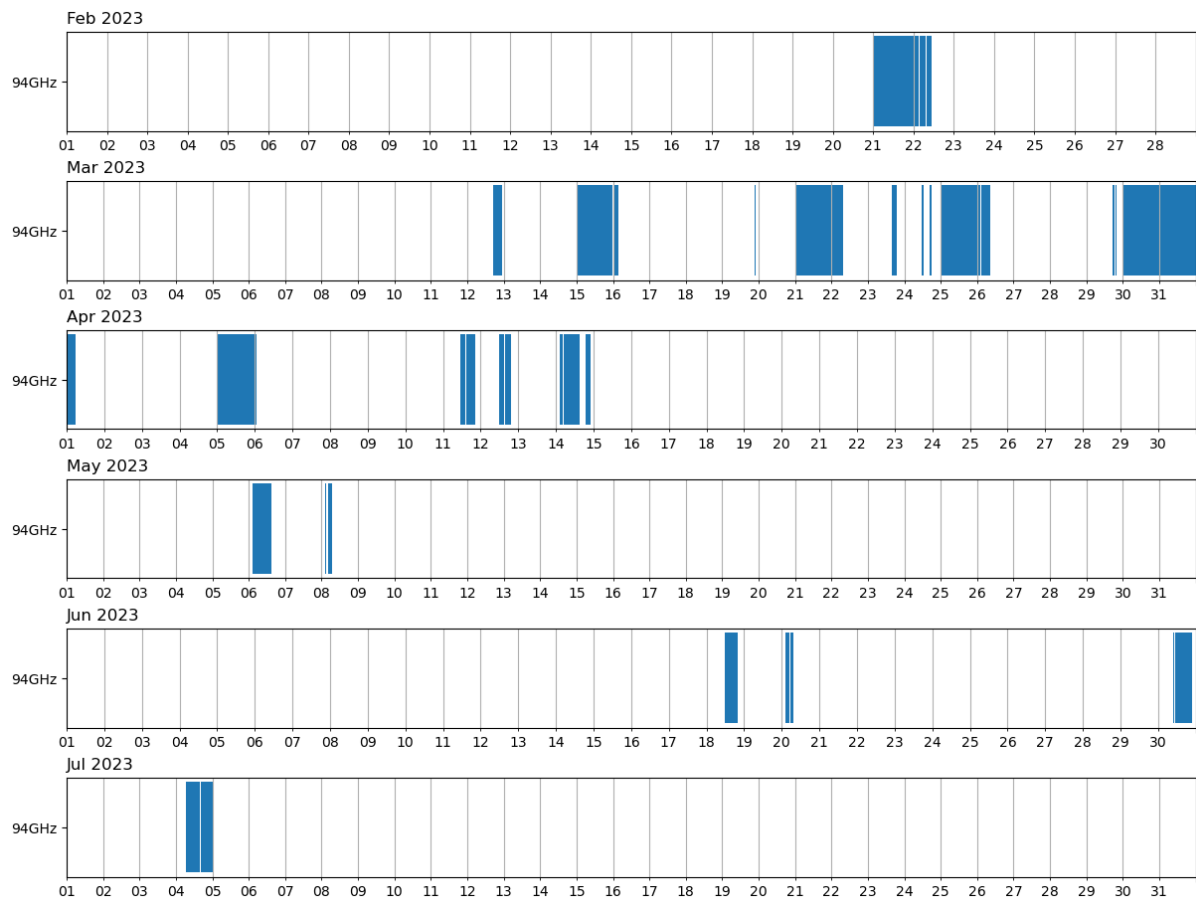


Figure 3: Summary of available time-series data

5. ANALYSIS

5.1 Abstract: The achievements of the tasks 3.4 to 3.13

In this WIVERN-EX-UK project tasks 3.4 to 3.8 and 3.13 involved analysis of radar observations made by the 94GHZ radar from the ground at Chilbolton to quantify the accuracy expected for the algorithms for deriving, winds, clouds and precipitation properties for the proposed WIVERN satellite. Tasks 3.9 to 3.12 carried out by the Politecnico Torino explored improvements of the E2E modelling.

The Chilbolton observations were made with the 94GHZ polarisation diversity radar transmitting pulse pairs alternately polarised H-V, V-H with the H and V pulses separated by 3km. Depolarising targets (e.g. the bright band) give rise to a “ghost”, but, as we shall see, these ghosts can be recognised and corrected. The ghosts result in a) a noisier line of sight wind (but no bias) and b) a positive bias for the reflectivity. Observations are reported with the radar vertically pointing and pointing at an angle of elevation 42 degrees as proposed for WIVERN.

Task 3.4 Analysis of H-V, V-H transmitted pulses pairs to identify any occasions when cross talk occurred resulting from ghost echoes and confirming that the ghost echoes affect only the leading or trailing H or V pulse and the unaffected pulse has the correct value of reflectivity.

Task 3.5 Verification that the theoretical formula predicting the loss of precision of the line-of-sight velocity is correct and the loss of precision can be estimated from the observed fall in the correlation of the H and V returns and there is no bias of the velocity.

Task 3.6. Statistics of the value of linear depolarisation (LDR) made at 42 degrees elevation show that LDR may be slightly larger than at vertical incidence. A statistical expression for the off-zenith value of LDR as a function of dBZ and T was obtained.

Task 3.7 Ghosts are observed frequently from the ground but, fortunately are much rarer from a satellite. This arises because the power from two targets of equal reflectivity separated by 3km is not the same at short ranges. For example, if there are two targets of the same Z, but for ranges of 1 and 4 km, the closer target will return a power that is $4^2 = 16$ or 12dB higher than for the more distant target. However, from the satellite the range is almost the same and over 650km so the power will be the same. But from the ground, if the close target is depolarising, then the power of the ghost from the close target will be 12dB greater than when observed from a satellite distance of 650km. This means that from the ground ghosts will be common and so their properties can be extensively analysed and a check made that the data degradation is as predicted by theory.

Task 3.8. Analysis of the CloudSat climatology of Z(reflectivity) profiles with the new off-zenith LDR climatology indicates slightly higher (less negative) values of LDR; these new values should be used for computing the frequency of ghosts observed by WIVERN which should be very slightly higher than would be the case at vertical incidence.

Task 3.9 (PoT). A method of obtaining the correct value of reflectivity even when ghosts are present is described, it relies on the fact that the ghost only appears for the trailing pulse.

Task 3.10 (PoT). Modelling results of the polarimetric signatures for different hydrometeor types at 94GHz.

Task 3.11 (PoT) Computation show a significant reduction of the depth of the blind zone with the WIVERN configuration rather than the vertical incidence for EarthCARE and CloudSat.

Tasks 3.12 (PoT) New observations at W-band with the Canadian aircraft of the magnitude of the surface return at various incidence angles for trees, dry snow, rocks and trees, so the depth of the blind zone close to the ground for WIVERN can be computed for these various surface types.

Task 3.13 Several WIVERN algorithms have been proposed for deriving ice water content (IWC) for every km along track from the differential phase shift between the H and V returns (PHIDP), and its change per km, KDP. However, WIVERN only transmits 12 pulse pairs per km, and this results in a phase noise of about 6 degrees in the observed values of PHIDP, and a

very noisy value of KDP and **so it will not be possible to implement this IWC algorithm in WIVERN**. Note that this level of phase noise **is acceptable** when considering the accuracy of the line of sight winds which is specified to be of 2m/s for 1km along track averaging. The folding velocity of 40m/s corresponds to a phase shift of ± 180 degs, so 6 degrees of noise in phidp is equivalent to $40 \times (6/180)$ which is approximately 1m/s and is acceptable

5.2 WIVERNEX-UK Detailed Abstract of Tasks 3.4 to 3.8

In this section provide more details of the analysis of ground observations at 94GHz made at Chilbolton looking upwards to characterise the ghosts. The ground observations comprise one second in “WIVERN” mode (H-V pulses separated by 20usec (3km) and a folding velocity of $800\text{um}/20\text{usec} = \pm 40\text{m/s}$. Each pulse pair is transmitted at $\sim 4\text{kHz}$ (separation 250usec, 37km). Depolarising hydrometeors resulted in ghost echoes at a distance 3km from the true target

The ground observations looking upwards comprise one second of H-V pulses with 20usec separation interleaved with one second observations **with three important additions:**

- a) Single transmitted pulses in H or V so the precise value of the LDR of the targets is known and the theoretical prediction of **the increased noise in the velocity estimate can be checked rather than using climatological values of LDR**.
- b) In addition, pulse pairs H and V separated by 160usec were transmitted so the “true velocity” could be measured directly, from the phase shift with a folding velocity of $800\text{um}/160\text{usec} = \pm 5\text{m/s}$
- c) From the ground looking upwards, ghosts are much more frequent than when observed from space. Consider two targets of equal Z, but at 1km and 4km range. The actual power returned from the target at 1km will be 16 times greater (12dB) than from the target at 4km and ghosts will be 12dB more intense than the same two targets observed from space at a range of 650km. Accordingly we can check the behaviour of these intense short- range ghosts and verify the theoretical expressions See explanation below.

FROM THE GROUND, LOOKING UPWARDS, A TARGET AT RANGE 1km will backscatter 16 times more power than the same target at 4km range. WIVERN: FROM SPACE THE SLANT RANGE OF THE TARGET ~ constant at 650km,

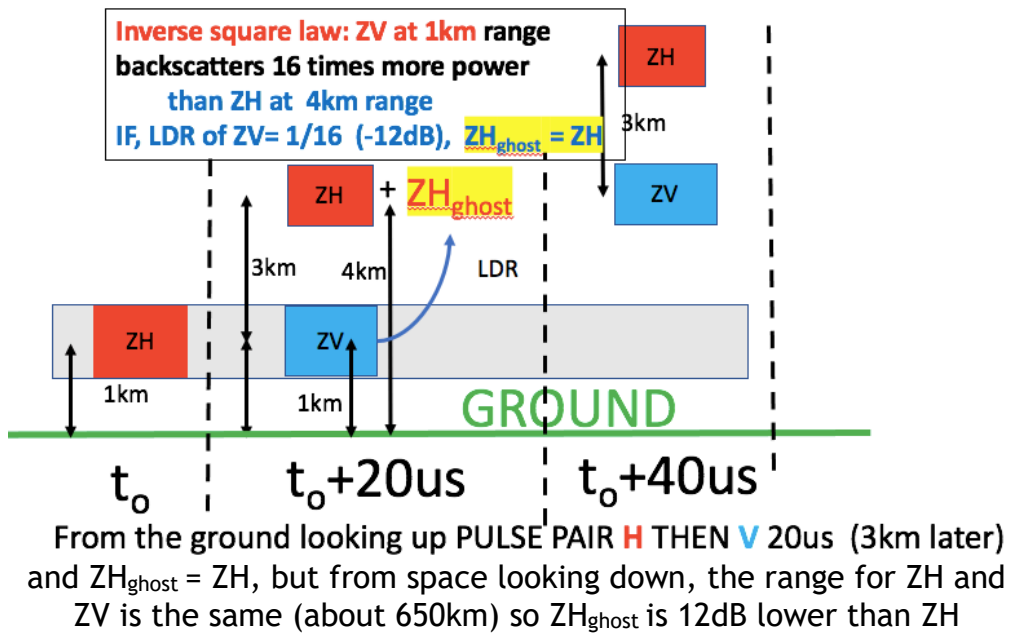


Figure 4: Diagram explaining the location and sizing of ghosts.

Task 3.4 Confirmation that the reflectivity bias affects only the leading pulse. Figure 5 (below) shows the reflectivity biases of 10dB for ghosts at 4km height produced from pulse at 1km height for 200,000 profiles observed on 21 Feb 2023 looking upwards. The LHS is the observed reflectivity of the ghost, and the RHS is the reflectivity of the ghost calculated from the observed LDR.

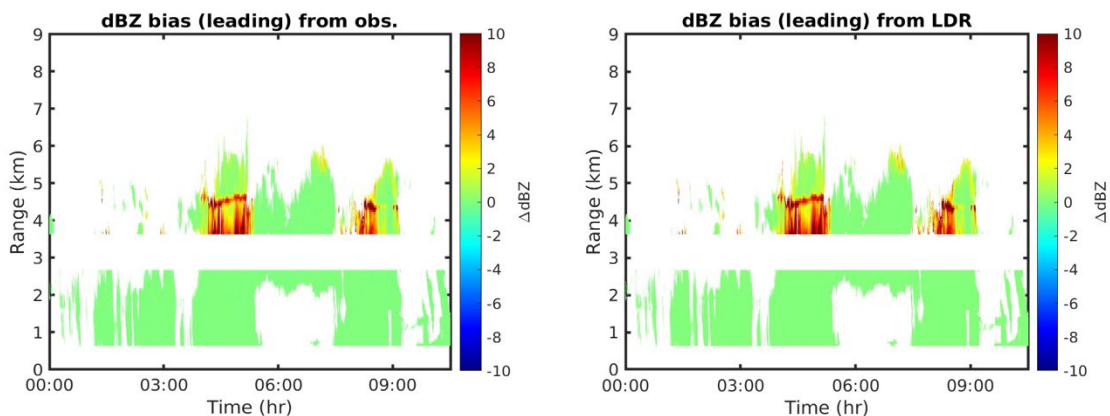


Figure 5: Reflectivity bias affecting the leading pulse, derived from the difference between double- and single-pulse reflectivity observations (LHS), and from single-pulse measurements of LDR shifted by 3km (RHS) from 22 February 2023 at vertical incidence.

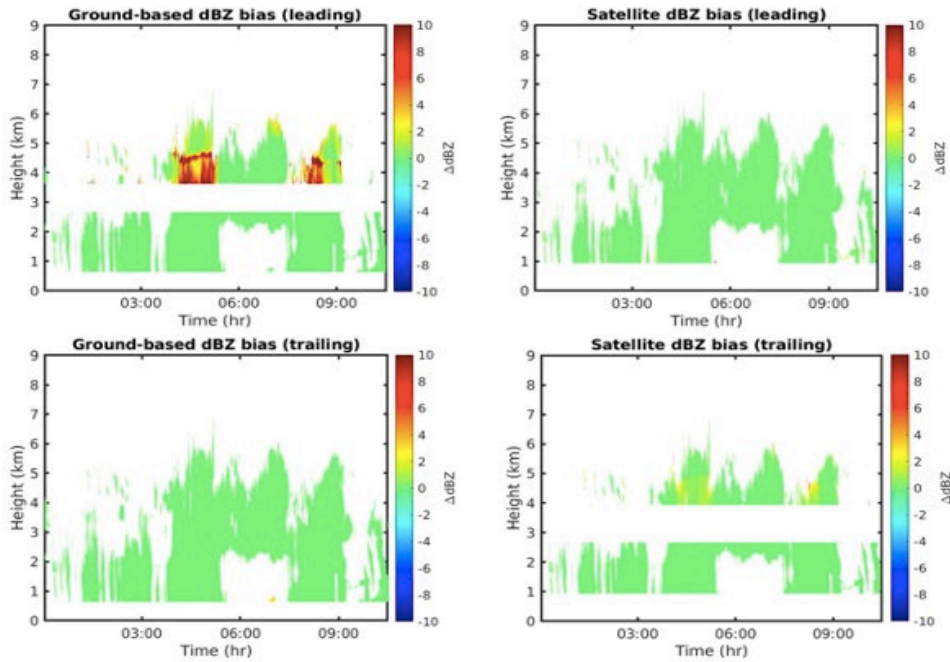


Figure 6: Reflectivity bias (due to ghost echoes) height-time plots from 22 February 2023 . Compares the ghosts that would be observed from the ground looking upwards (LHS) with those that would be observed by WIVERN looking (downwards). Ghosts are absent for the trailing pulse from the ground and for the leading pulse observed from space. Observed from the ground (lower LHS) and at WIVERN resolution (4 min. x 660m) and as would be observed from satellite looking down (upper RHS).

Task 3.5. Verification that the theoretical formula predicting the loss of precision of the line-of-sight velocity is correct and the loss of precision can be estimated from the observed fall in the correlation and the signal to ghost ratio and there is no bias of the velocity estimate.

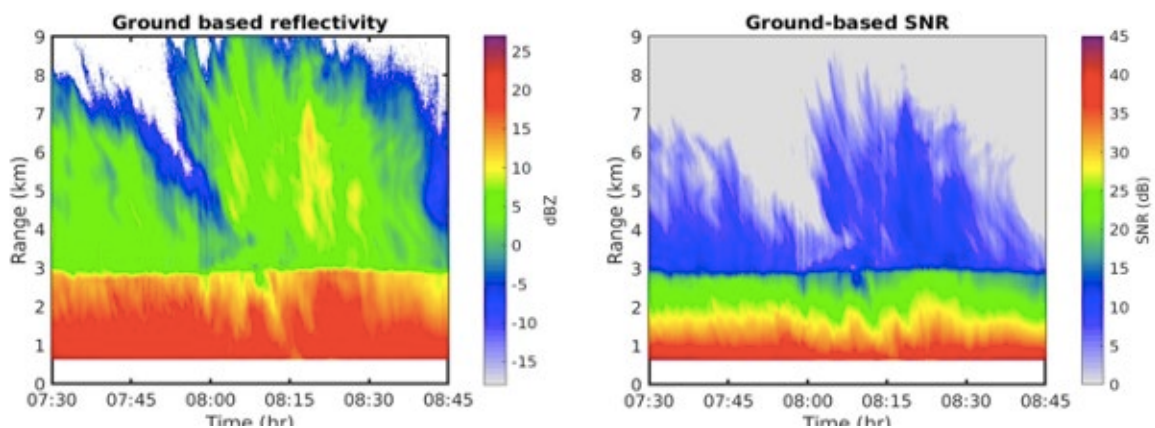


Figure 7: Observations from the ground looking up: 6 May 2023 at an elevation angle of 48°. LHS: true reflectivity profile. RHS: The SNR profile observed from the ground; for the same Z at a range of 1 and 4 km the SNR is 16 times lower at a range of 4km.

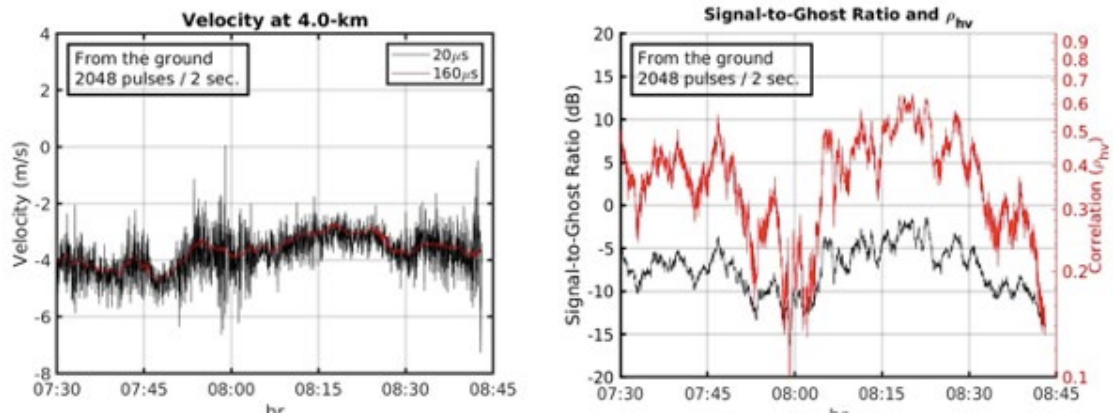


Figure 8: The ghost produced at a range of 4km from the return at 1km range. LHS: The noisy velocity at a range of 4km where there is a ghost produced from the echo at 1km range, the red line is the “true” value of the velocity. RHS: Values of SGR (black) from the ghost at 4km range. The SGR is between -5 and -10dB, (i.e. ghost 10 times the original signal). The observed correlation of the H and V returns is typically 0.4 and falls as low as 0.2.

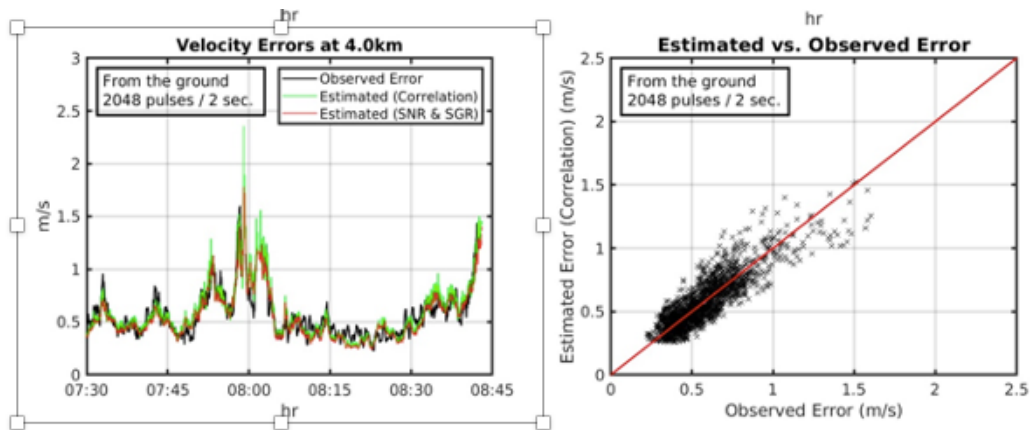


Figure 9: Confirmation that the random noise in the velocity estimate can be derived from the lowering of the correlation of the H and V returns. LHS – the random errors of the velocity at 4km height affected by the ghost can reach 1.5m/s where the SGR ratio is very low. BLACK – the observed value of the random error of the derived velocity at 4km height. GREEN - the predicted random error of the velocity based on the observed drop in correlation RED - random error of the velocity derived from SNR and SGR.

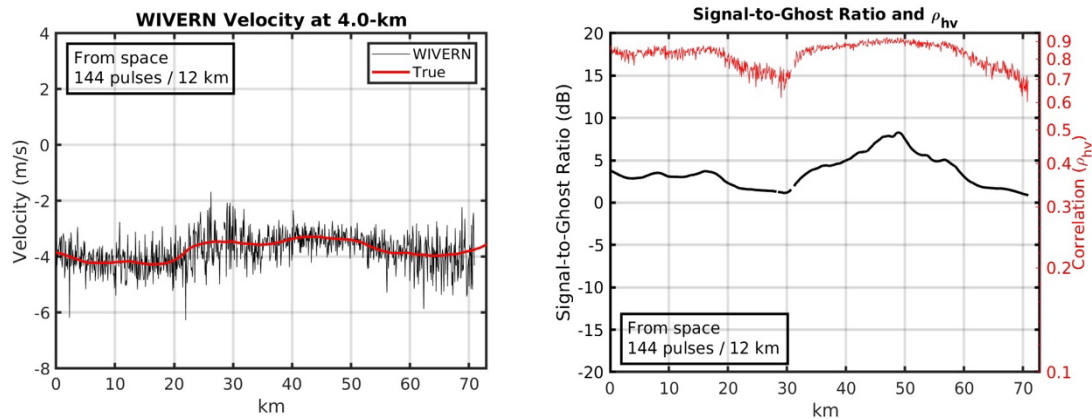


Fig 10: The data in Fig 1 for 6 May 2023 at an elevation angle of 48° as would be observed from WIVERN at a range of 650km. In this case the large change in SNR when the range changes from 1 to 4km is absent and the ghost is much reduced. LHS: BLACK the rms uncertainty of the ghost at 4km height as would be observed by WIVERN at a range of 650km. RED – the true velocity at 4km height. RHS: SGR of the ghost is now about 5dB, i.e. the signal is three times the value of the ghost (rather than 5 times less (-7dB) in Fig 2) and the correlation only falls to 0.7 (rather than 0.2)

Task 3.6. Statistics of the values of linear depolarisation (LDR) made at 42 degrees elevation show that LDR be slightly larger than at vertical incidence. A statistical expression for the off-zenith values of LDR as a function of Z and T was obtained.

The frequency of occurrence of ghost echoes will depend upon that values of LDR expected in rain, the melting layer, and in the ice. Previous work had been carried out at vertical incidence. At vertical incidence a finite value of LDR arises because the mean shape of the hydrometeors is not spherical, but the hydrometeors are oblate spheroids (e.g. melting snowflakes) with their major axis aligned in the horizontal. However, WIVERN has an incidence angle of 42 degs, so, if the hydrometeors (e.g. melting snowflakes have a spread of canting angles, then the values of LDR may be slightly higher at 42deg incidence than at vertical.

Table 3: LDR quantiles (10%, 25%, 50%, 75% and 90%) for various height bands for satellite observations at vertical incidence. ECMWF freezing level height corrected based on the height of maximum LDR.

Satellite	10%	25%	50%	75%	90%
-25°C	-20.5	-20.4	-20.1	-19.7	-19.5
-20°C	-20.5	-20.2	-19.9	-19.7	-19.5
-15°C	-20.3	-20.1	-19.8	-19.7	-19.5
-10°C	-20.3	-20.1	-19.8	-19.6	-19.3
-5°C	-20.3	-20.0	-19.7	-19.4	-19.0
0°C	-20.1	-18.8	-17.1	-15.6	-14.4
5°C	-21.0	-20.9	-20.8	-20.7	-20.5

Table 4: LDR quantiles (10%, 25%, 50%, 75% and 90%) for various height bands for satellite observations at 48° elevation.

Satellite	10%	25%	50%	75%	90%
-25°C	-	-	-	-	-
-20°C	-	-	-	-	-
-15°C	-19.6	-19.5	-19.4	-19.1	-19.0
-10°C	-19.9	-19.7	-19.4	-19.2	-18.9
-5°C	-19.8	-19.6	-19.3	-18.8	-18.5
0°C	-18.5	-17.0	-15.2	-13.9	-12.9
5°C	-20.8	-20.8	-20.6	-20.5	-20.4

1. That in rain (5 degC) the values of LDR at about -20.5 to -20.9 dB are almost identical. This is limited by the isolation of the antenna.
2. At 0deg C (the bright band) the values of LDR at 48deg incidence are about 2dB higher at the WIVERN 48deg elevation than at vertical.
3. In the ice (-10 to -15C) the LDR values at the Wivern angle are about 0.4dB higher than at vertical incidence.

These values should be used for predicting the occurrence of ghosts from the CloudSAT observations

Task 3.7. Calculations on the frequency of ghosts as observed from the ground and compared with the expected frequency from space.

For Task 3.4, it was shown that the impact of ghost echoes was significantly different for the leading and trailing pulses, and also markedly different for ground-based and satellite observations based on a single example (22 February 2023). Now, results are aggregated over all cases at vertical incidence. Figure 1 shows the distribution of SGR for the leading (top row) and trailing (bottom row) for ground-based (LHS) and satellite (RHS) observations.

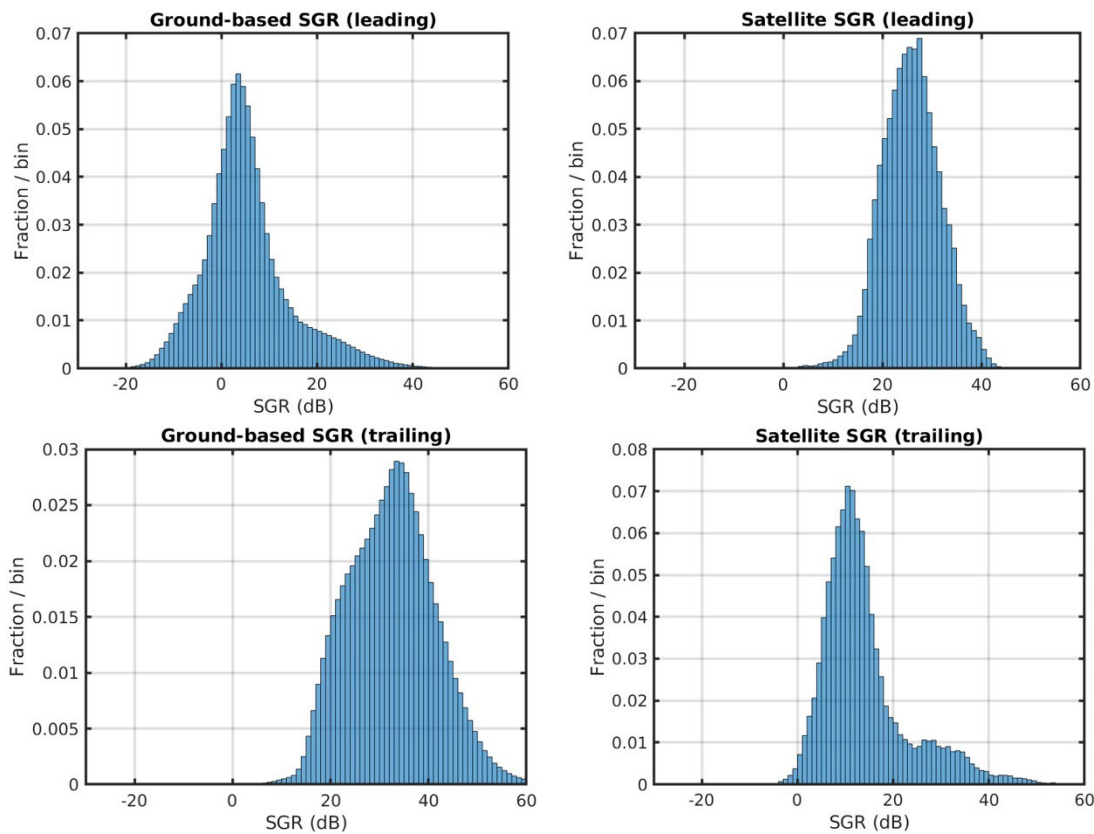


Figure 11: Histograms of SGR for the leading (top row) and trailing (bottom row) for ground-based (LHS) and satellite (RHS) observations based on observations over 15 days (1-dB bins). Note that the number of occasions with values of SGR exceeding 10dB, that is to say the ghost is equal to 10% of the total signal, is very low for the leading pulse for the satellite (top RHS) and for the trailing pulse for the ground-based observation geometry (bottom LHS).

WIVERN: Reflectivity errors are minimal for WIVERN using the leading pulse and from the ground using the trailing pulse.

Figure 12 displays the corresponding plots of reflectivity biases due to ghost echoes are shown with bin widths of 0.25 dB.

RHS (top) confirms that reflectivity biases are absent from space using the leading.

LHS (bottom) confirms that reflectivity biases are absent from space using the trailing pulse.

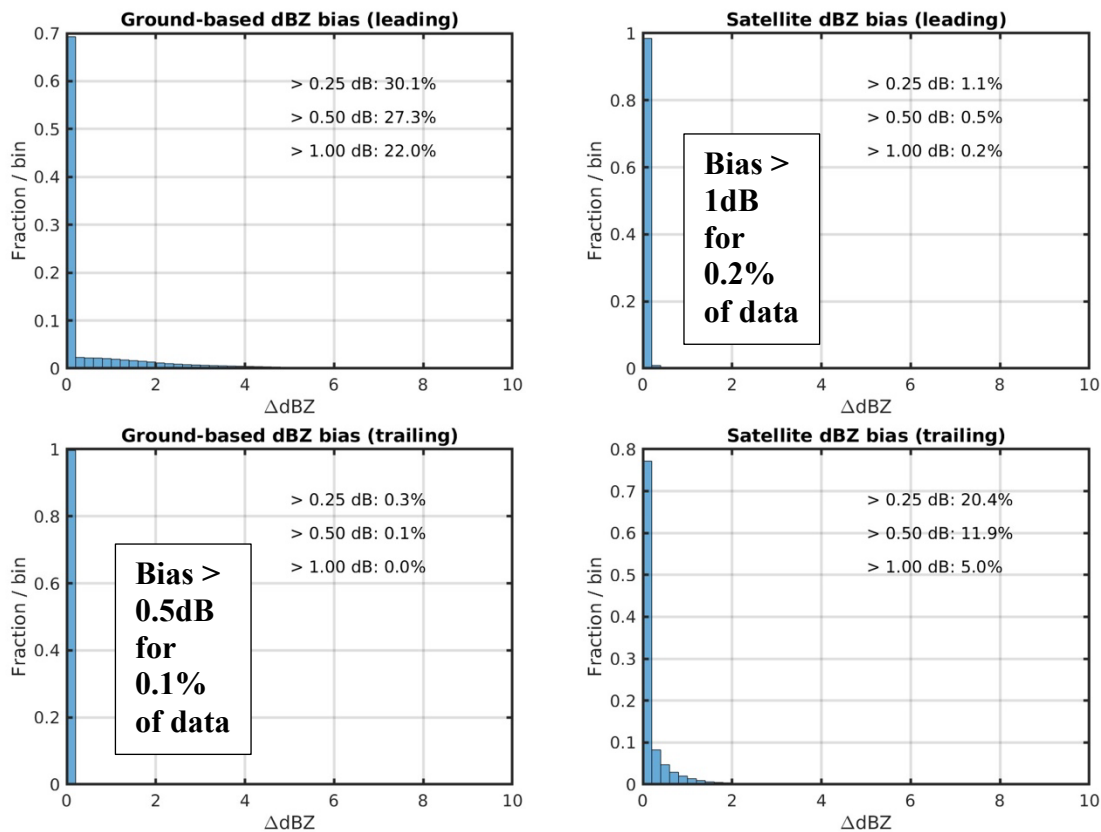


Figure 12: Histograms of reflectivity biases due to ghost echoes for the leading (top row) and trailing (bottom row) for ground-based (LHS) and satellite (RHS) observations based on all observations at vertical incidence (0.2-dB bins).

Calculation on the frequency of ghosts as observed from the ground and their comparison with the expected frequency from space. Ghosts are observed frequently from the ground but are much rarer from a satellite. This arises because the power from two targets of equal reflectivity separated by 3km distance is not the same. For example, if there are two targets of the same Z, but at ranges of 1 and 4 km, then the closer target will return a power that is $4 \times 4 = 16$ or 12dB higher than the more distant target. From the satellite the range is almost the same and over 650km so the power will be the same. But from the ground, if the close target is depolarising, then the power of the ghost from the close target will be 12dB greater than when observed from the satellite at a distance of 650km. This means that from the ground ghosts will be common and their properties can be better observed

Task 3.8. Revisit the Cloudsat Z profile climatology to better predict the frequency of ghosts and the ability to recover the true reflectivity.

It was shown in Task 3.7 that the leading pulse of the pulse pair from the WIVERN satellite is only weakly impacted by ghost echoes. The reflectivity climatology from CloudSat has been used to investigate the prevalence of ghost echoes affecting the leading pulse. A simple model of linear depolarisation ratio (LDR) based on observations at 48° elevation (presented in Task 3.6) is shown in Figure 13. A constant lapse rate of 6°C/km has been assumed to express LDR as a function of height above the freezing level.

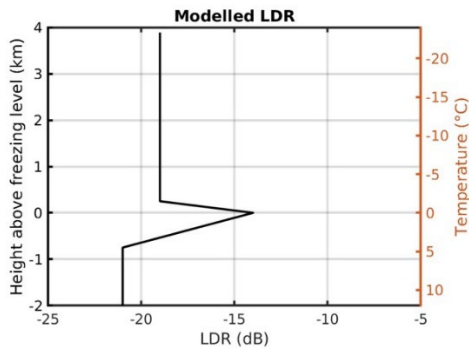


Figure 13: Modelled LDR profile relative to the freezing level height for a lapse rate of 6°C/km).

The next stage is to calculate the frequency of occurrence of reflectivity greater than various thresholds for 1km horizontal integration are shown in Fig 2 and are represented as functions of height for the Tropics (between 30°S and 30°N) and for Mid-latitudes (between 30°N and 60°N, and between 60°S and 30°S).

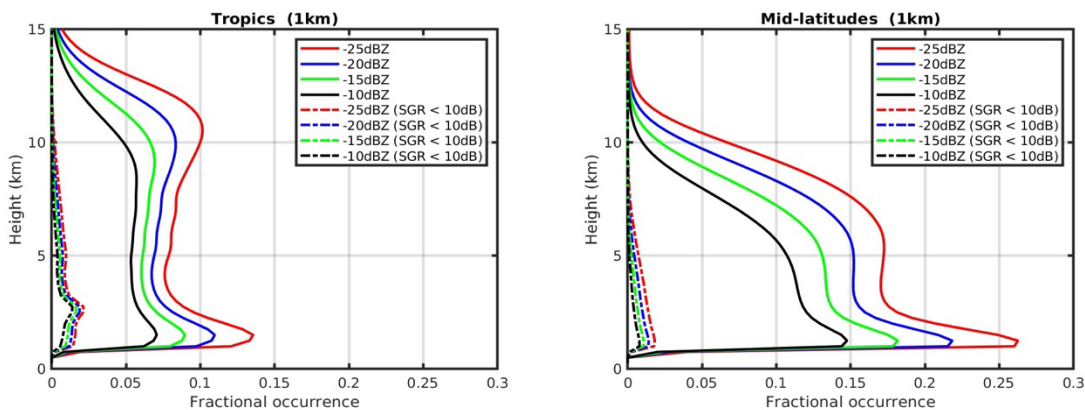


Figure 14: Solid coloured lines. Frequency of occurrence above reflectivity threshold (-25dBZ, -20dBZ, -15 dBZ and -10dBZ) from CloudSat in the Tropics (LHS between -30° and 30° latitude): and (RHS) Mid-latitudes (between latitudes of ± 30°- 60°: RHS); both with 1km horizontal integration.

Dashed coloured line: frequency of occasions with a given reflectivity dBZ threshold that there is a ghost at a given height with an SGR < 10dB using the LDR profiles in Fig. 1 and the Cloudsat data base. An SGR < 10dB leads to a reflectivity bias < 0.4dBZ.

Note that ghosts are rare occurring 1% of the time near the melting layer bright band and <<1% away from the melting layer, whereas clouds are present about 10% of the time in the tropics.

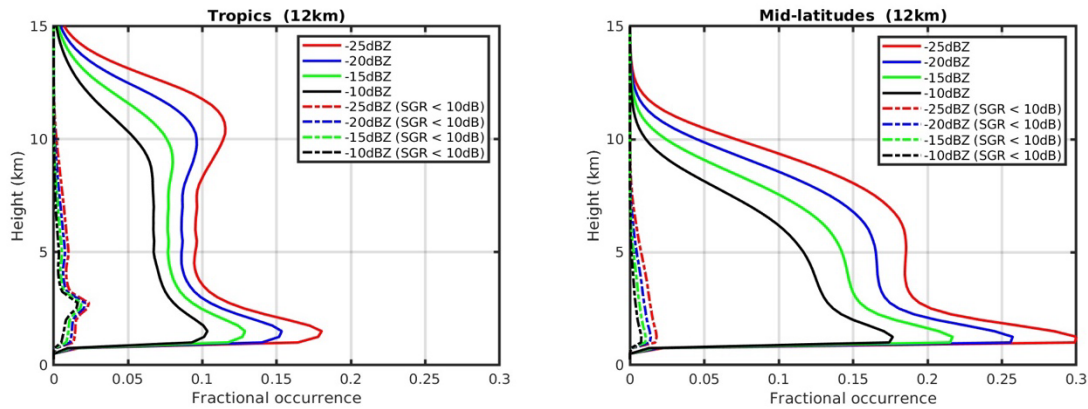


Figure 15: As for Fig 2 but with 20-km integration rather than 1km so the data are representative of the large-scale flow and are suitable for data assimilation. The dashed curves are much closer to the y axis than in Fig 2. The occurrence of ghosts is drastically reduced when the data are averaged over 20km. The only naturally occurring features with high, persistent and horizontally extensive LDR are the bright band (melting layer) and the surface of the Earth.

CONCLUSION: For use in data assimilation, the WIVERN wind data should be averaged over 20km in the horizontal so they are representative of the large-scale flow. This will remove many ghosts that occurred for 1km horizontal integration, apart from those due to a) persistent bright bands/melting layers or b) depolarisation due to the Earth’s surface. The winds from these few remaining ghosts will not be biased but will be noisier. Biases in the reflectivity can be minimised by using the returns from the leading pulse (see Task 3.7).

6. DATA PRODUCTS

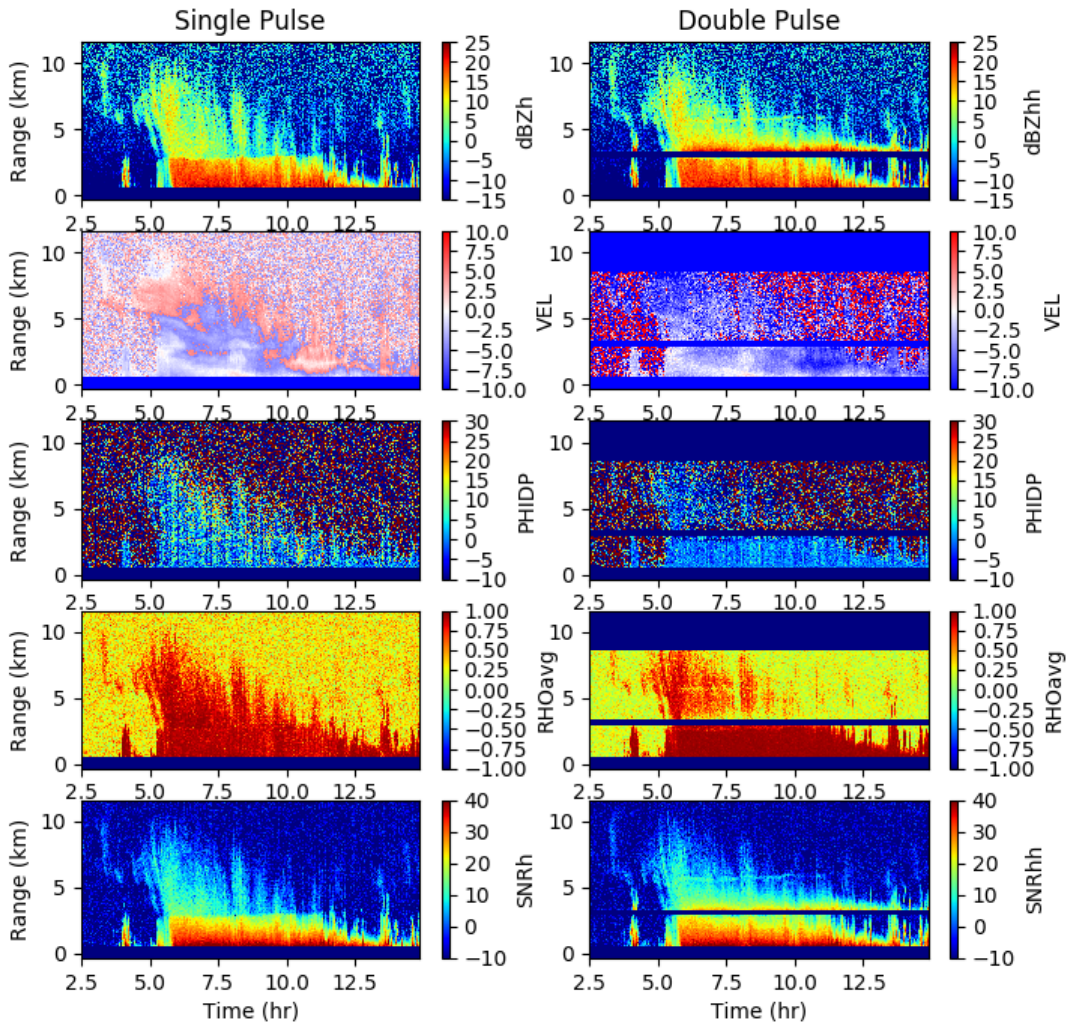
Level 2 data for the Galileo radar at chilbolton dataset from phases 1 and 2 as described in section 4 is presented in netCDF format. The 20 case days listed in tables 1 (at vertical incidence) and 2 (at 42° incidence). Each case is processed for single and double pulse formats and with 5 different averaging periods for pulses per ray, 12, 48, 144, 2048, 6144, resulting in 10 files per day. The data is organised and parameters are provided in arrays with dimension of time and range, these parameters are listed in table 5.

Table 5: Level 2 data parameters for the Galileo radar dataset taken at Chilbolton

Variable	Long name	unit	Single pulse	Double pulse
dBZh	Radar reflectivity at horizontal polarisation	dBZ	X	
dBZhh	Radar reflectivity at horizontal polarisation (leading pulse H)	dBZ		X
dBZv	Radar reflectivity at horizontal polarisation	dBZ	X	
dBZvv	Radar reflectivity at vertical polarisation (leading pulse V)	dBZ		X
dBZhv	Radar reflectivity at vertical polarisation (leading pulse H)	dBZ		X
dBZvh	Radar reflectivity at horizontal polarisation (leading pulse V)	dBZ		X
ZDR	Differential radar reflectivity	dB	X	
LDR	Linear depolarisation ratio (calibrated)	dB	X	
VEL	Doppler velocity	m/s	X	X
PHIDP	Differential phase shift	°	X	X
RHOavg	Correlation coefficient (average)	n/a	X	X
SNRh	Signal-to-noise ratio at horizontal polarisation	dB	X	
SNRhh	Signal-to-noise ratio at horizontal polarisation (leading pulse H)	dB		X
SNRv	Signal-to-noise ratio at vertical polarisation	dB	X	
SNRvv	Signal-to-noise ratio at vertical polarisation (leading pulse V)	dB		X
SNRhv	Signal-to-noise ratio at vertical polarisation (leading pulse H)	dB		X
SNRvh	Signal-to-noise ratio at horizontal polarisation (leading pulse V)	dB		X
SGRh1	Signal-to-ghost ratio of leading pulse at horizontal polarisation	dB	X	
SGRv1	Signal-to-ghost ratio of leading pulse at vertical polarisation	dB	X	
SGRh2	Signal-to-ghost ratio of trailing pulse at horizontal polarisation	dB	X	
SGRv2	Signal-to-ghost ratio of trailing pulse at vertical polarisation	dB	X	

A simple python 2.7 script has been provided which loads the data to python dictionaries and plots the basic variables from a chosen case and pulse setting, comparing the single and double pulsed versions – changing the date and pulse per ray should be trivial at the start of the program. An example of the quicklooks generated is see in figure 16.

20230506 - 48° elevaion - 12 pulses per ray



Quicklook of level 2 data with 12 pulses per ray on May 6th, 2023.